Neuro-Oncology
24(5), 726–738, 2022 | https://doi.org/10.1093/neuonc/noab264 | Advance Access date 19 November 2021

Real-time evaluation of glioblastoma growth in patient-specific zebrafish xenografts

Elin Almstedt[†], Emil Rosén[†], Marleen Gloger, Rebecka Stockgard, Neda Hekmati, Katarzyna Koltowska, Cecilia Krona, and Sven Nelander

Department of Immunology, Genetics and Pathology, Uppsala University, Uppsala, Sweden (E.A., E.R., M.G., R.S., N.H., K.K., C.K., S.N.)

Corresponding Author: Sven Nelander, PhD, Department of Immunology, Genetics, and Pathology, ag Hammarskjölds väg 20, E-751 85 Uppsala, Sweden (sven.nelander@igp.uu.se).

[†]These authors share co-authorship for this work.

Abstract

Background. Patient-derived xenograft (PDX) models of glioblastoma (GBM) are a central tool for neuro-oncology research and drug development, enabling the detection of patient-specific differences in growth, and *in vivo* drug response. However, existing PDX models are not well suited for large-scale or automated studies. Thus, here, we investigate if a fast zebrafish-based PDX model, supported by longitudinal, AI-driven image analysis, can recapitulate key aspects of glioblastoma growth and enable case-comparative drug testing.

Methods. We engrafted 11 GFP-tagged patient-derived GBM IDH wild-type cell cultures (PDCs) into 1-day-old zebrafish embryos, and monitored fish with 96-well live microscopy and convolutional neural network analysis. Using light-sheet imaging of whole embryos, we analyzed further the invasive growth of tumor cells.

Results. Our pipeline enables automatic and robust longitudinal observation of tumor growth and survival of individual fish. The 11 PDCs expressed growth, invasion and survival heterogeneity, and tumor initiation correlated strongly with matched mouse PDX counterparts (Spearman $R = 0.89$, $p < 0.001$). Three PDCs showed a high degree of association between grafted tumor cells and host blood vessels, suggesting a perivascular invasion phenotype. *In vivo* evaluation of the drug marizomib, currently in clinical trials for GBM, showed an effect on fish survival corresponding to PDC *in vitro* and *in vivo* marizomib sensitivity.

Conclusions. Zebrafish xenografts of GBM, monitored by AI methods in an automated process, present a scalable alternative to mouse xenograft models for the study of glioblastoma tumor initiation, growth, and invasion, applicable to patient-specific drug evaluation.

Key Points

1. A high-throughput, patient-comparative, *in vivo* model of glioblastoma.
2. A neural network quantifies tumor growth over time in freely swimming zebrafish.
3. Very effective analysis of tumor growth and survival in treated and untreated fish.

Despite decades of research, the identification of drugs to treat glioblastoma (GBM) is still moving slowly. To accelerate progress, it is important to establish patient-specific models of tumor growth and drug treatment that are well suited for large-scale investigation. Today, mouse-based flank and orthotopic PDX models are commonly applied in neuro-oncology to assess patient differences in tumor growth, treatment efficacy, and drug

Importance of the Study

One of the central challenges of neuro-oncological investigation is to accurately model patient differences in glioblastoma growth, invasion, and drug response. The current standard model for this is patient-derived xenograft models in mice. Such mouse models, however, are costly, time-consuming, and do not enable observation of the growth of the tumor in living tissue. Here, we establish that a comparatively simple patient-derived zebrafish xenograft model provides a promising alternative. The model that we describe is implemented in a high-throughput format and uses an AI technique (convolutional neural networks) to monitor tumor growth in freely swimming fish. The results thus provide a scalable alternative to existing mouse models for translational studies of glioblastoma growth, invasion, and drug response.

toxicity.[1–8] However, mouse models are not practical in settings that require substantial numbers of treatments or large collections of patient-derived samples. This motivates research to identify effective, alternative *in vivo* models of GBM.

Recently, zebrafish (*Danio rerio*) embryo xenografts have shown promise in experimental oncology as a model for tumor growth, and treatment response.[9–11] In studies of carcinomas, zebrafish patient-derived xenografts (zPDX), where patient cells are injected into embryos 2–6 days post-fertilization (dpf), exhibit patient-specific differences in treatment response.[12,13] It is therefore interesting to consider embryonic zPDX models for translational studies of nervous system cancers. Notably, the nervous system makes up a large part of the early zebrafish embryo, and zebrafish have detectable blood-brain barrier function already 3 dpf, as shown by the exclusion of doxorubicin from brain parenchyma.[14] Transparent zebrafish strains such as roy-/-, nacre -/- *casper* zebrafish enable microscopic monitoring of tumors,[15] whereby fluorescently tagged tumor cells can be tracked by epifluorescence, confocal or light-sheet microscopy. Initial studies of GBM transplanted into zebrafish indicate that the cells form tumors, which suggests a possible model for drug evaluation.[16–18] However, systematic characterization of glioblastoma zPDX models with accurate longitudinal observation has not been described in a scalable format.

Here, we report a scalable procedure for the evaluation of patient-specific tumor growth, survival, and treatment response in zebrafish grafted with patient-derived GBM cells (PDCs). Our method integrates live fluorescence monitoring of freely swimming fish with image analysis by a deep convolutional neural network (CNN), thus enabling the automated generation of longitudinal tumor data without any manual monitoring. We characterize the growth rate and survival of 11 patient-derived IDH wild-type cell cultures from our Human Glioma Cell Culture biobank.[7,19,20] Comparing the results in zebrafish to matched mouse xenograft counterparts, we note a significant agreement between tumor growth and initiation. Using light-sheet imaging of whole embryos, we further characterize the invasion of the PDCs and identify cell cultures suited for studies of GBM invasion in zebrafish. Together, our results provide a fast way of assessing GBM tumor initiation capacity, invasion, and drug response *in vivo,* and thereby a scalable complement to current mouse-based PDX systems.

Materials and Methods

GFP-Tagged Patient-derived Cell Cultures

Patient-derived glioblastoma cell cultures (PDCs) labeled with Green Fluorescent Protein (GFP) and luciferase (pBMN(CMV-copGFP-Luc2-Puro), Addgene plasmid #80389) and patient data for each PDC were acquired from the Human Glioma Cell Culture consortium[7,19,20] and maintained as previously described.[7,21] HGCC sample collection was approved by the Uppsala regional ethical review board (2007/353); informed consent was obtained from all subjects included. The cells were cultured in neural stem cell (NSC) media (DMEM/F12 (1:1) w/ Glutamax, Neurobasal (Life Technologies), 1X N-2, 1X B-27 (ThermoScientific), 1% penicillin/streptomycin, and supplemented with 10 ng/ml EGF and 10 ng/ml FGF (Peprotech) in a humidified atmosphere on laminin-coated (Sigma) primaria plates (Corning) at 37°C with 5% CO2, and split using StemPro Accutase (Thermo Scientific). The cell cultures used were U3008MG-GFP-luc, U3013MG-GFP-luc, U3017MG-GFP-luc, U3051MG-GFP-luc, U3054MG-GFP-luc, U3137MG-GFP-luc, U3173MG-GFP-luc, U3179MG-GFP-luc, U3180MG-GFP-luc, U3213MG-GFP-luc, U3291MG-GFP-luc. For brevity of presentation, the cultures are mentioned without their GFP-luc tag throughout the manuscript.

Zebrafish and Xenotransplantation

Animal experiments were approved by the regional animal ethics board (C68/15, 5.8.1-08213/2017, 5.8.18-09077-2020, EP 161/14, 5.8.18-10590/2018) and complied with Swedish regulations for animal testing. Adult *casper*[15] and *Tg(kdrl:Hsa.HRAS-mCherry)s916*,[22] zebrafish were kept in the SciLifeLab zebrafish facility at Uppsala University (http://www.scilifelab.se/facilities/zebrafish/). Fertilized eggs were obtained from natural spawning. Embryos were kept at 28°C in methylene blue-containing water until injection. We prepared cells and performed xenotransplantations as described.[23,24] Sub-confluent cells were detached using StemPro Accutase (Thermo Scientific), passed through a 40–70 µm nylon mesh (Sigma-Aldrich), and resuspended in NSC medium containing polyvinylpyrrolidone (PVP; 20 mg/ml, Sigma #PVP360), and kept on ice until transplantation. For transplantations, 1 dpf embryos were dechorionated

using 1 mg/ml pronase (Sigma) and anesthetized with 0.6 mM tricane. Before injections, cells were concentrated by spinning down, removing almost all media, and re-suspended. Cells were back-loaded into pulled (Narishige PC-10) glass capillaries (Narishige GD-1) and injected using a pneumatic microinjector (Narishige IM-31 or Pneumatic Picopump PV820), the volume adjusted to contain approximately 150 cells/injection. For U3180MG and U3213MG, additional injections with 50 cells were made. Xenografted zebrafish were kept in 100 µL E3 media with 25 mM HEPES (E3/H) in 96-well plates at 33°C in a humidified atmosphere. At 5 dpf, zebrafish were sacrificed with 2.4 mM tricane.

Real-Time Image Acquisition

Xenotransplanted embryos were transferred in 100 µL E3/H to 96-well plates and loaded into the IncuCyte S3 (Sartorius). Phase and fluorescence images were acquired every 4–6 h from approximately 30 hpf to 120 hpf using the whole well mode (4X objective). Phase (8-bit) and fluorescent (16-bit) TIFF images were exported for every time point. Tumor localization was analyzed in 88 randomly chosen fish from 6 independent experiments (n = 14–15/experiment) and categorized into forebrain, midbrain, hindbrain,[25] combinations thereof, or outside CNS.

Image Semantic Segmentation

The integrated intensity was measured from the fluorescent channel. A CNN, based on the U-Net architecture[26] (Supplementary Material) and trained on manually labeled images, was used to identify tumor cells. It was implemented in Python 3.5.3 using Keras 2.1.6[27] with Tensorflow 1.8.0[28] as the backend and trained to distinguish between background, well-edge, egg yolk, eye, tumor, fish body, dead fish, and image artifacts. The artifact class contained blurry, partial, and out-of-focus fish. Before segmentation, each image was reduced to 1800 x 1800 pixels (50% reduction) and split into 512 pixel square tiles with 256 pixels overlap. Tiles were segmented individually and then stitched together. Training images (n = 155) were created manually using similar 512 x 512 patches and were chosen to reflect different states of the well and fish.

Additional Image Data Processing

Prior to the estimation of survival, growth, and treatment responses, the data underwent additional filtering. First, some images showed erroneous tumors due to image artifacts or dying fish. A second classifier classified each image as either Valid (valid image of tumor), Invalid (image artifacts, such as duplicated fish) or Dead (image of dead fish) (Supplementary Material). Dead or Invalid images were not used to estimate tumor growth. 215 images were manually labeled in order to evaluate the method. Second, the background fluorescent signal was removed from each well. Background intensity was computed as the average image, excluding images with dead fish and pixels classified as egg yolk or tumor. Third, fish with 5 or fewer valid images were removed. Fourth, fish with zero signal in at least 3 valid time points, out of the first 5 time points, were removed, as the injection probably had failed (Supplementary Material).

Survival Analysis

Survival was determined as follows. For each well we find τ such that $\sum_{t=0}^{T} |H(t-\tau) - Y_t|$ is minimized, where τ is the time of death, T is the number of images, H(.) is the Heaviside function and Y_t is the vital status at time t. Y_t is 1 for images classified as dead, otherwise 0. If $\tau > T$ the fish survived until the study endpoint and the event is censored. We performed survival analysis using Cox proportional hazard regression in Python 3.6 with Lifelines v0.14.4.[29] Model comparisons were done using the likelihood ratio test.

Statistical Model of Growth Rate and Treatment Effects

Tumor expansion and growth can be estimated in each fish from the (exponential) increase or decrease in tumor area and GFP-signal. Due to multiple longitudinal measurements per fish, we implemented the following hierarchical model,

$$\log(Y_i, t) \sim 1 + t + t:\gamma + (1 + t + t:\gamma || batch). \quad (1)$$

where Y_i, t is the measurement of fish i at time t and γ is 1 for treated fish and 0 otherwise. Batch indicates the group-level effects of individual batches of injections. With the exception of 4 PDC injected twice, each batch represents a single PDC. To obtain posterior distributions of γ and t in (2) we used the No-U-turn sampler[30] with an uninformative prior. The model was implemented in Python 3.6 using PyMC3 3.6[31] (Supplementary Material).

Drug Treatment

Marizomib (Sigma-Aldrich) was diluted in a 2X concentration in E3/H containing 10 µM dexamethasone, the standard treatment to reduce edema in GBM,[32] and added in 100 µL to embryos (to a final concentration 0.2 µM, total volume of 200 µL). Controls contained identical concentrations of DMSO (0.02%) and dexamethasone.

Light-Sheet Microscopy/ 3D-Image Acquisition

We obtained fluorescence images of the zebrafish xenografts with a light-sheet microscope (Leica TCS SP8 DLS or Zeiss Z.1) at 5 dpf (invasion characterization) or 2 and 5 dpf (volumetric measurements). For Zeiss Z.1, we embedded whole fish in 1% low-melting agarose in a glass capillary. For Leica TCS SP8 DLS, we mounted whole zebrafish in 1% low-melting agarose within a 1.5 mm U-shaped glass capillary, glued to the center of a glass bottom dish (35 mm, Greiner Bio-One). Imaging chambers were filled with E3/H containing 0.6 mM tricane. We imaged whole zebrafish heads with a 10x/0.3W DLS objective (Carl Zeiss) plus DLS TwinFlect 5 mm water mirror cap on a Leica TCS SP8

DLS microscope (Leica Microsystems) by z-stack across the full depth of the head. Identical image acquisition settings were applied for all zebrafish, including controls. The light-sheet thickness was 4.8 µm, the z-step size was set to 3.7 µm, with system-optimized settings for 3D-merging for a total of 100-150 images (=slices) per z-stack.

EdU Immunohistochemistry

To visualize 5-ethynyl-2′-deoxyuridine (EdU) incorporation in S-phase cells, we used the Click-iT® RNA Alexa Fluor®594 kit (ThermoFisher) following the manufacturer's instructions with the following modifications. Zebrafish embryos at 5 dpf were treated with 500 µM EdU with 10% DMSO in embryo medium for 3 hours at 33°C on a shaker. We fixed embryos in 4% PFA overnight at 4°C, mounted embryo heads in Omnipaque solution (350 mg I/ml iohexol, GE Healthcare), and obtained images on a Leica TCS SP8 confocal microscope.

Caspase Immunohistochemistry

Embryo whole-mount immunohistochemistry, including the Proteinase K treatment, was performed as described.[33,34] Primary antibodies were anti-GFP (chicken, 1:400, ab13970); anti-cleaved Caspase3 (1:500, rabbit, Abcam, ab13847). Secondary antibodies were anti-chicken IgG (1:400, Alexa 488; Jackson Immuno Research, 703-545-155) and anti-rabbit IgG-HRP (1:1000, Cell Signalling, 7074). Embryo heads were mounted in Omnipaque (350 mg I/ml iohexol, GE Healthcare) and imaged on a confocal microscope (Leica TCS SP8).

Image Analysis

To evaluate tumor growth and tumor-vessel interactions, we used LasX (Leica Microsystems), Imaris (Bitplane), and Fiji[35] software. Fiji and Imaris were used to adjust brightness, contrast, channel deconvolution, surface rendering and masking of the GFP-channel, z-stack maximum intensity projects, and z-stack videos. From the projections, we categorized the tumor invasion phenotypes (1 = extensive invasion, 0.5 = intermediate, 0 = no invasion) for each PDC. Individual slices of the z-stacks of each xenograft were visually examined to identify tumor-vessel interactions (Supplemental videos). Tumor volumes were measured in Imaris (Bitplane) by rendering the surface of the GFP-channel with consistent detail size and intensity threshold settings; significance of volume increase was calculated using paired t-tests (GraphPad Prism).

Mouse Xenograft Tumor Initiation

All 11 PDCs in this study have been orthotopically injected in mice, as part of the ongoing characterization of the HGCC biobank (C Krona, et al., unpublished results). Six of these PDCs initiated tumor growth, whereas the other five did not (Table 1, $n \geq 4$/ PDC).

Results

High-Throughput Pipeline to Measure Real-Time Glioblastoma Growth In Vivo

This study aimed to characterize the growth of glioblastoma PDCs in the developing zebrafish brain and to

Table 1. Characteristics of 11 Injected PDCs

Patient-derived glioblastoma cell culture	Clinical data			Cellular data			
	Age	Survival	Sex	Doubling time	Subtype	Proteasome inhibitor	Mouse tumor initiation **
	years	days	F = female M = male	hours		0 = resistant 1 = sensitive	0 = no 1 = yes
U3008MG	64	38	F	51	MES	0	0
U3013MG	78	122	F	38	PN	1	1
U3017MG	68	442	M	na	PN + CL	1	0
U3051MG	72	444	M	na	MES	na	1
U3054MG*	60	611	F	31	PN + MES	1	1
U3137MG	74	847	M	101	MES	1	0
U3173MG	73	229	F	na	MES	0	0
U3179MG*	63	474	M	na	CL	1	1
U3180MG	80	267	M	40	PN + CL	0	1
U3213MG	77	133	F	63	MES	0	0
U3291MG	60	206	F	na	CL	na	1

PDCs have been molecularly characterized regarding gene expression (RNAseq), mutations (exome sequencing), methylation (Illumina 450 array), and copy number alterations.[20] *Recurrent tumor **Krona et al, unpublished data.

establish a robust high-throughput method to measure *in vivo* outcomes (Figure 1A). In current protocols for the analysis of zebrafish tumor xenografts, the process of imaging is time-consuming, as it involves tranquilization and mounting fish (e.g. in agarose) to control their orientation.[14,17] While this helps the user to determine the tumor localization and spread, it reduces the number of individuals that can be analyzed in a reasonable time. We, therefore, considered an alternative method based on live monitoring of fluorescent signals from GFP-tagged GBM cells in freely moving fish. We reasoned that such live monitoring would increase the number of observation timepoints, thereby enabling accurate measurements of tumor growth. Injection of 150 cells into the midbrain of each embryo at 24-30 hours post-fertilization (93% success rate with a confirmed brain localization, predominantly in the midbrain, Supplementary Figure 1A) and incubation of the fish in a real-time imaging system (IncuCyte S3) collecting one image every 4-6 hours over 4 days, we could evaluate tumor growth in 576 individuals with minimal handling.

To enable an accurate analysis of all images (~9000), we opted for a CNN. Unlike existing methods, we designed it to identify the tumor location, fish location, and vital status of the fish in each image. It does so by classifying all parts of the image into one of eight different classes (Figure 1B). This, in turn, allows us to follow tumor growth (GFP-signal), tumor expansion (tumor area), and survival (vital status) for each fish.

We conducted several analyses to ensure that the image analysis was robust. Problems that we identified were related to moving fish leading to duplicates, missing or out-of-focus fish, and dead fish. To solve this, our image analysis pipeline was also designed to classify images as Valid, Dead, or Invalid. When compared to an independent set of 255 manually labeled images, we achieved good agreement (77%), typically erring on the conservative side, by flagging valid images as invalid (Figure 1C and D). A large part of the wrongly classified images were cases where the fish showed early signs of death, which the CNN had difficulty identifying. In these cases, the estimated survival would be delayed until the visual signs of fish death were more obvious.

Altogether, longitudinal imaging of live fish, combined with semantic segmentation enabled us to measure tumor growth and classify fish survival with accuracy, in a highly automated fashion.

Patient-Specific Differences in Xenograft Growth and Zebrafish Survival

Next, we applied our pipeline to 11 well-characterized glioblastoma PDCs transduced to express GFP stably (Supplementary Figure 1B). The PDCs were selected from the HGCC resource[7,20] to represent different molecular subtypes, robust *in vitro* growth, and available data on tumor initiation in mice (Table 1). We estimated the tumor cell proliferation rate and survival time for each fish (Figure 2A and B, Supplementary Figure 2). To validate these results, we performed light-sheet microscopy to determine tumor volume increase over time (Figure 2C–F). EdU staining detected 6-16% proliferative cells (Figure 2G–H), and only a small fraction of apoptotic cells as judged by cleaved Caspase3 staining (Supplementary Figure 6D).

Having established that the GFP-signal increase correlated with tumor volume, we estimated growth in each fish, assuming exponential growth. We utilized a Bayesian method, from which we obtained a posterior distribution of the growth rate (Figure 3A), given as a 95% highest posterior density (HPD) interval (i.e. a Bayesian version of a traditional confidence interval). Growing tumors would thus have a positive growth rate while a negative growth rate indicates a regressing tumor. We saw substantial differences in proliferative capacity, ranging from rapid exponential growth (U3013MG, 95% HPD: 37–54% daily signal increase) to decline of signal (e.g. U3008MG, 95% HPD: 31–39% daily signal decrease). The growth rate was in general positively correlated with the number of injected cells (R = 0.36, 95% CI [0.23-0.47]), indicating a density-dependent growth effect (a.k.a Allee effect; Supplementary Figures 3A–B, 4A–C). Moreover, survival differed between the PDCs ($p < .001$, Figure 3B), and a higher proliferation rate predicted shorter survival ($p = .002$, Figure 3C). Combining all covariates, we noted that the PDC-specific and growth rate effects on survival were independent of each other ($p = .01$, Supplementary Material). This suggests that there is a patient-specific effect on survival that is unrelated to proliferation.

Our analysis supported that the assay is robust. GFP-measurements were consistent with microscopy data and PDC survival, growth estimates were consistent between independent batches (Figure 3A–B) and similar results were obtained when using tumor area instead of integrated intensity (Supplementary Figure 3C). We conclude that the proposed assay can yield robust estimates of tumor growth in zebrafish that differ between individual PDCs, and which are associated with fish survival.

Zebrafish Xenografts Predict Tumor Initiation in Mice

To compare outcomes in zebrafish with outcomes in mice, we obtained data from an ongoing characterization of the HGCC biobank by orthotopic injection into adult, immunodeficient mice.[7,19,20,36] Among the 11 PDCs, six initiated tumors ($n >= 4$ per PDC). Similarly, we computed initiation in zebrafish as the number of fish with positive proliferation. We found that we could perfectly separate tumor and non-tumor initiating PDCs in mice, using the *in vivo* estimated zebrafish growth rate for each PDCs (Spearman R = 0.89, $p < .001$) (Figure 3D). This suggests that our model can serve as an alternative to mouse experiments to establish tumor initiation ability, a proxy for cancer cell stemness.

Zebrafish Xenografts Show Patient-Dependent Differences in Invasive Growth

GBMs invade surrounding tissue via several anatomical routes, including invasion along white matter tracts, in the perivascular compartment, and through gray matter.[37–40] In addition, a distinction between single-cell and collective invasion has been proposed.[41] We therefore asked if such

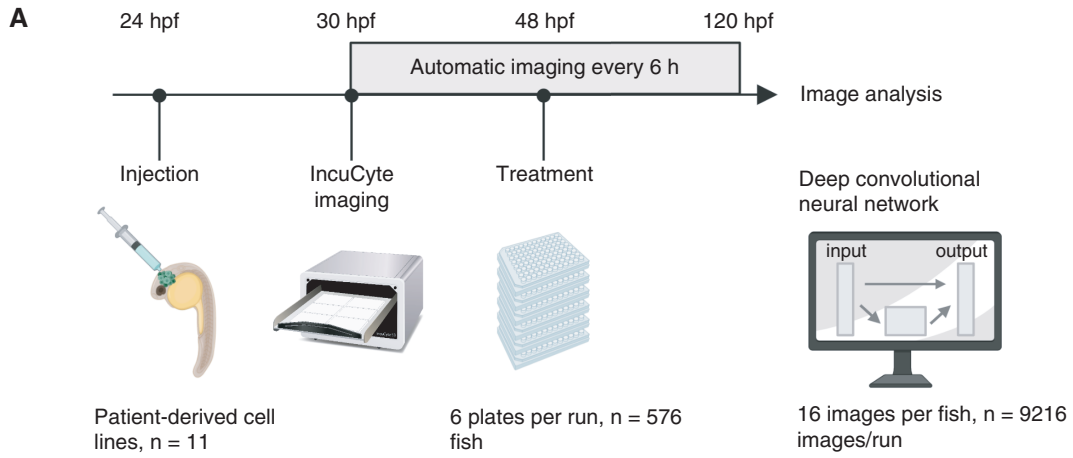

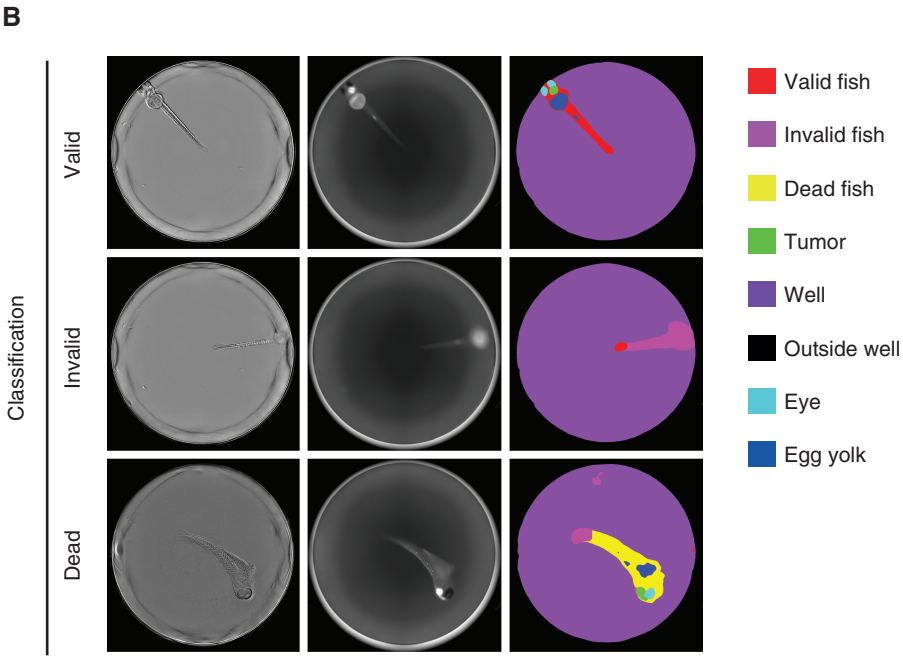

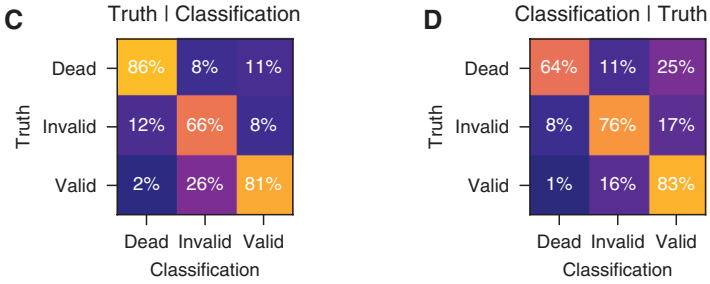

Figure 1. Zebrafish xenografted with patient-derived cells (PDCs) can be monitored in real-time using automatic imaging and image analysis. (A) Experiment workflow. High-throughput injection of GFP-tagged PDCs can be monitored in real-time in six 96-well plates using the IncuCyte S3. (B) Pixel-wise semantic segmentation for tumor localization and post-classification of image types. Left panel: Bright Field; Middle panel: Green Fluorescence; Right panel: post-classification. (C and D) Confusion matrices of post-segmentation image classifications for precision (C) and sensitivity (D).

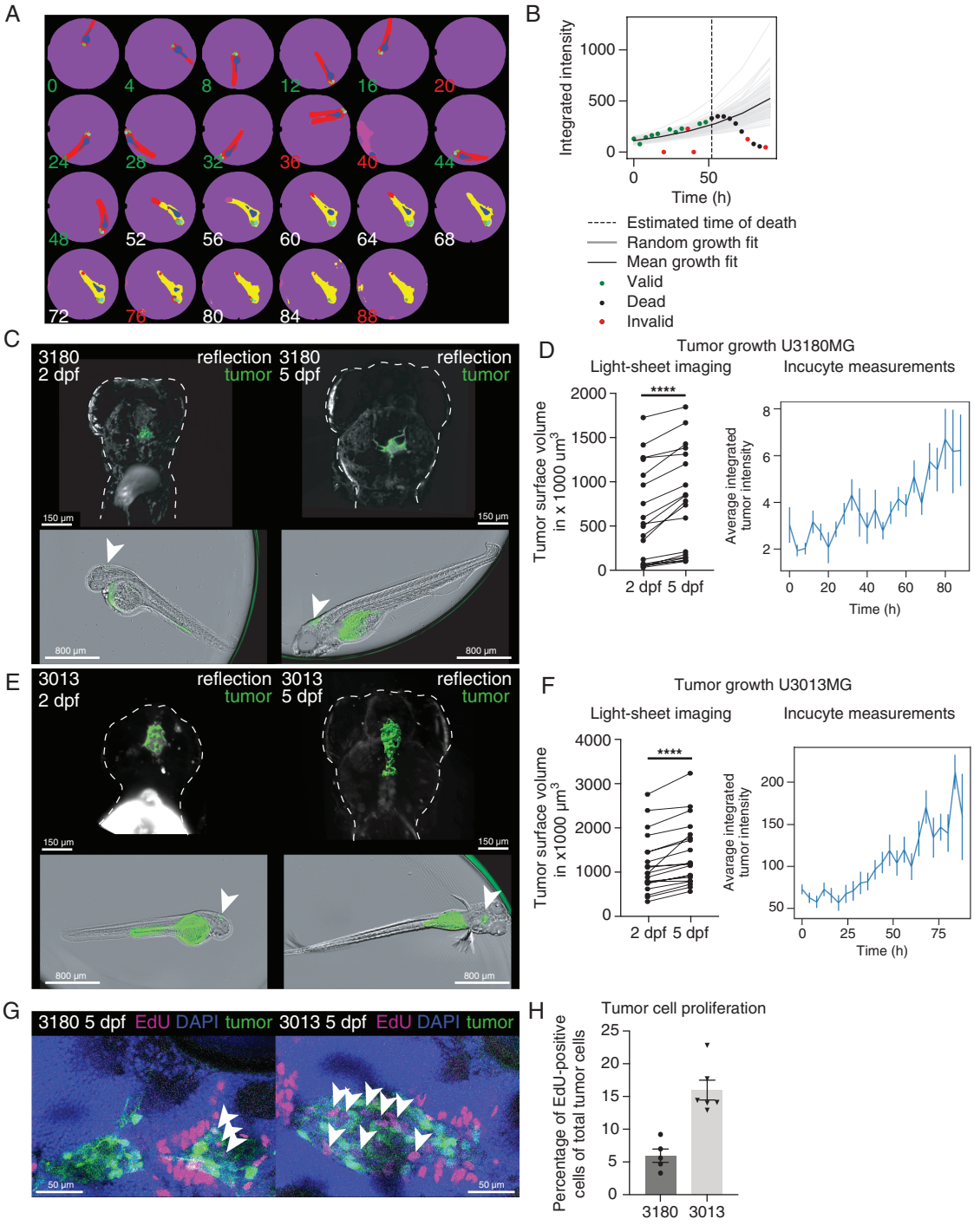

Figure 2. GFP-signal measurements are representative of tumor growth. (A) Segmented time series of one representative U3013MG xenograft. Numbers indicate time (in hours) and each image is classified as Valid (green number), Invalid (red number), or Dead (white number). (B) Estimates of exponential tumor growth estimated from (A). (C) and (E) Representative light-sheet and IncuCyte images of U3180MG and U3013MG tumors (green) in zebrafish at 2 and 5 dpf. (D) and (F) Correlating tumor growth measurements of rendered surface volume ($n = 20$/ PDC, $p < .0001$ paired t-test) and IncuCyte measurements ($n = 144$/PDC). (G) Confocal projections showing cell nuclei (DAPI, blue), EdU staining (magenta), and tumor cells (GFP, green) injected into zebrafish at 5 dpf. Arrows indicate proliferative tumor cells. (H) Quantification of the EdU and GFP-positive tumor cell ratio at 5 dpf ($n = 6$/PDC).

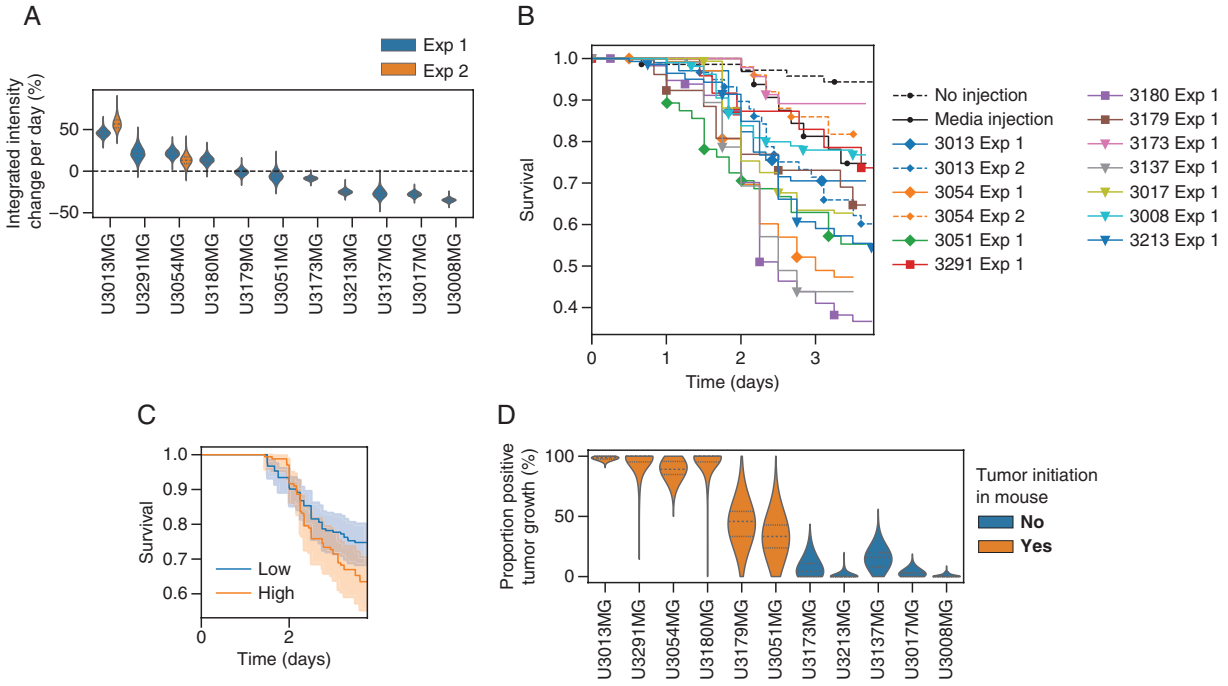

Figure 3. Patient-derived cells (PDC) specific *in vivo* growth and survival. (A) Posterior distribution of PDC-specific proliferation rate. (B) PDC-specific effect on survival compared with negative control. (Rhombus: proliferative, Square: invasive, Triangle: non-proliferative). (C) Survival stratified by *in vivo* tumor proliferation. (D) Posterior distribution of tumor initiation capacity, compared to tumor initiation in orthotopic mouse xenografts.

patterns of invasive growth were present in the zebrafish xenografts.

To evaluate the invasive properties in relation to the brain vasculature, we injected each PDC into *Tg(kdrl:mCherry)* zebrafish, which express a red fluorescent protein in vascular endothelial cells, driven by the promoter of the zebrafish homolog of the VEGF2 receptor, *kdrl*. We visualized the tumors and vasculature using light-sheet microscopy at single-cell resolution (Figure 4, Supplementary Figure 5, Supplementary Videos 1–11).

We could observe three main patterns. In one set of highly invasive PDCs (U3179MG, U3180MG, U3291MG), we observed a mixture of singular and collectively invading cells, predominantly in association to the vasculature. In a second set of PDCs, invasion was moderate and dominated by collective invasion (U3008MG, U3013MG, U3054MG, U3137MG). A third group showed no signs of invasion (U3017MG, U3051MG, U3173MG, U3213MG) (Figure 4B–C, Supplementary Figure 5C). We noted that U3179MG, while not having a clear increase in tumor signal, was still highly invasive, compared with other PDCs with low growth rate. In the U3179MG xenografts, we noted that while integrated intensity did not increase over time, the tumor area did (Supplementary Figure 3C). This indicates that tumor area could potentially be used to measure invasiveness directly.

We conclude that our patient-derived zebrafish xenografts exhibit differences in tumor invasion, with possible differences in singular and collective invasion and blood vessel association. This suggests that zPDXs could be a tool to study differences in cellular growth and behavior as well as interactions between GBM cells and vasculature in an *in vivo* setting.

Patient-Specific Differences Responses to Marizomib Treatment

Last, we evaluated if our model could be used to distinguish patient-specific treatment effects. In a recent *in vitro* drug screen on 100 PDCs, we identified a heterogeneous response to proteasome inhibitors.[20] We therefore chose to evaluate differential responses to marizomib, a proteasome inhibitor currently in clinical trials for glioblastoma (clinicaltrials.gov: NCT03345095). We selected the three zPDXs (U3013MG, U3054MG, U3180MG) that were both represented in the previous drug screen and highly proliferative in zebrafish (Figure 5A–B). Among these, U3013MG and U3054 are sensitive to proteasome inhibitors *in vitro*, whereas U3180MG is resistant.[20] Consistent with these previous data, we detected a significant survival effect in treated U3013MG (74%, 95% CI [4.7–93%] lower hazard ratio, $p = 0.042$) and non-significant effect in U3054MG (67%, 95% CI [–7% to 90%] lower hazard ratio, $p = 0.065$), while there was no survival benefit for the resistant PDC U3180MG (Figure 5C). Combining the p-value for the two sensitive PDCs[20] using Fisher's method, we find that the combined p-value is 0.027, indicating an overall significant

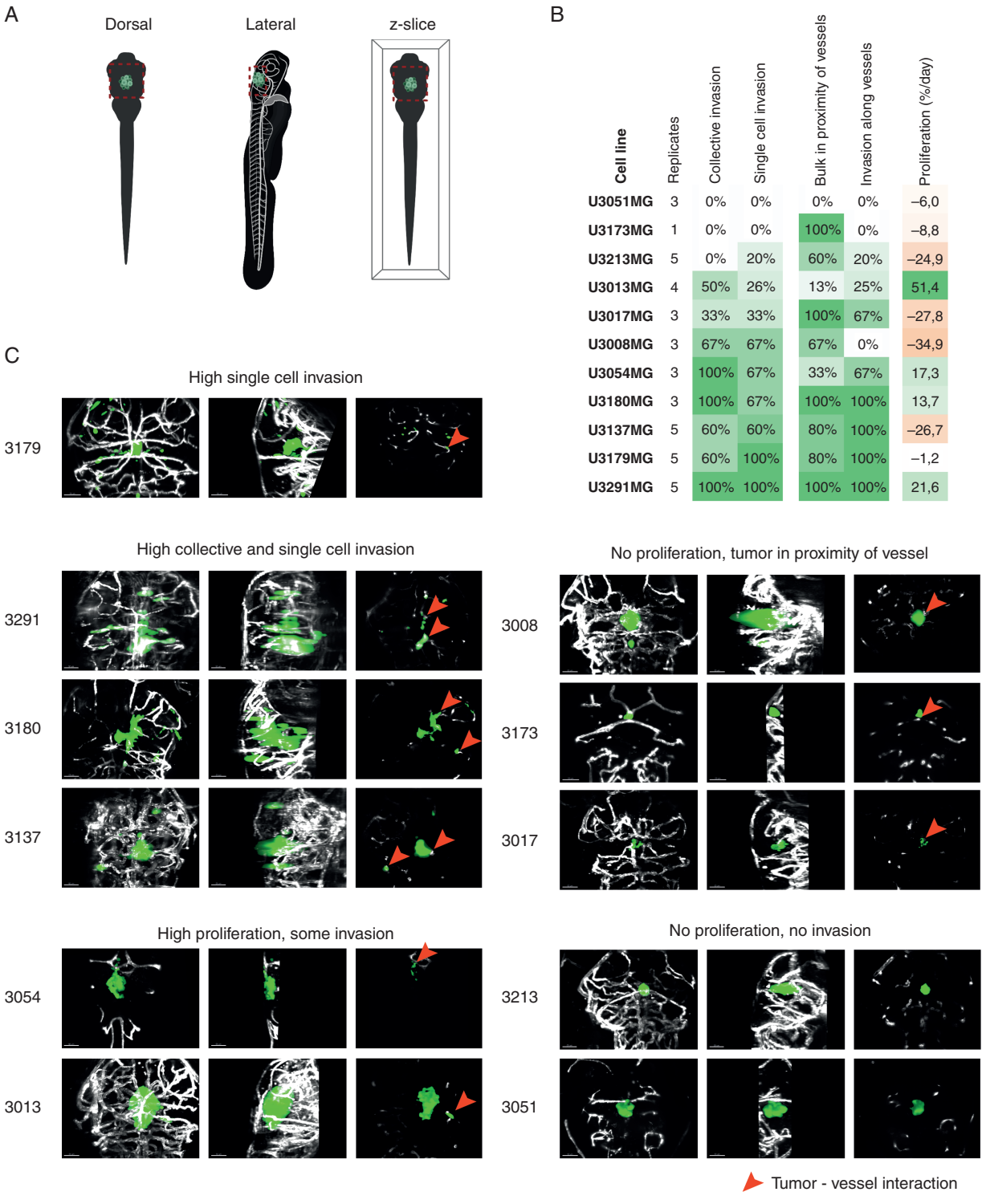

Figure 4. Patient-derived glioblastoma cells (PDC) show heterogenous growth and invasion patterns. (A) Illustration of images in (C). (B) Quantified *in vivo* characteristics for 11 PDCs. (C) Representative light-sheet (maximum projection) images of the different growth patterns for 11 PDCs in live zebrafish at 5dpf. Left: dorsal; middle: lateral; right: z-slice. Green = GFP, white = mCherry. Scale bars = 50 um.

survival benefit for marizomib in PDCs that are sensitive to proteasome inhibitors *in vitro*. However, we did not find a reduction in tumor growth (Figure 5B).

To support future drug testing studies, we also estimated the statistical power of our method. Given our experimental setup, at least a 17% daily decrease in

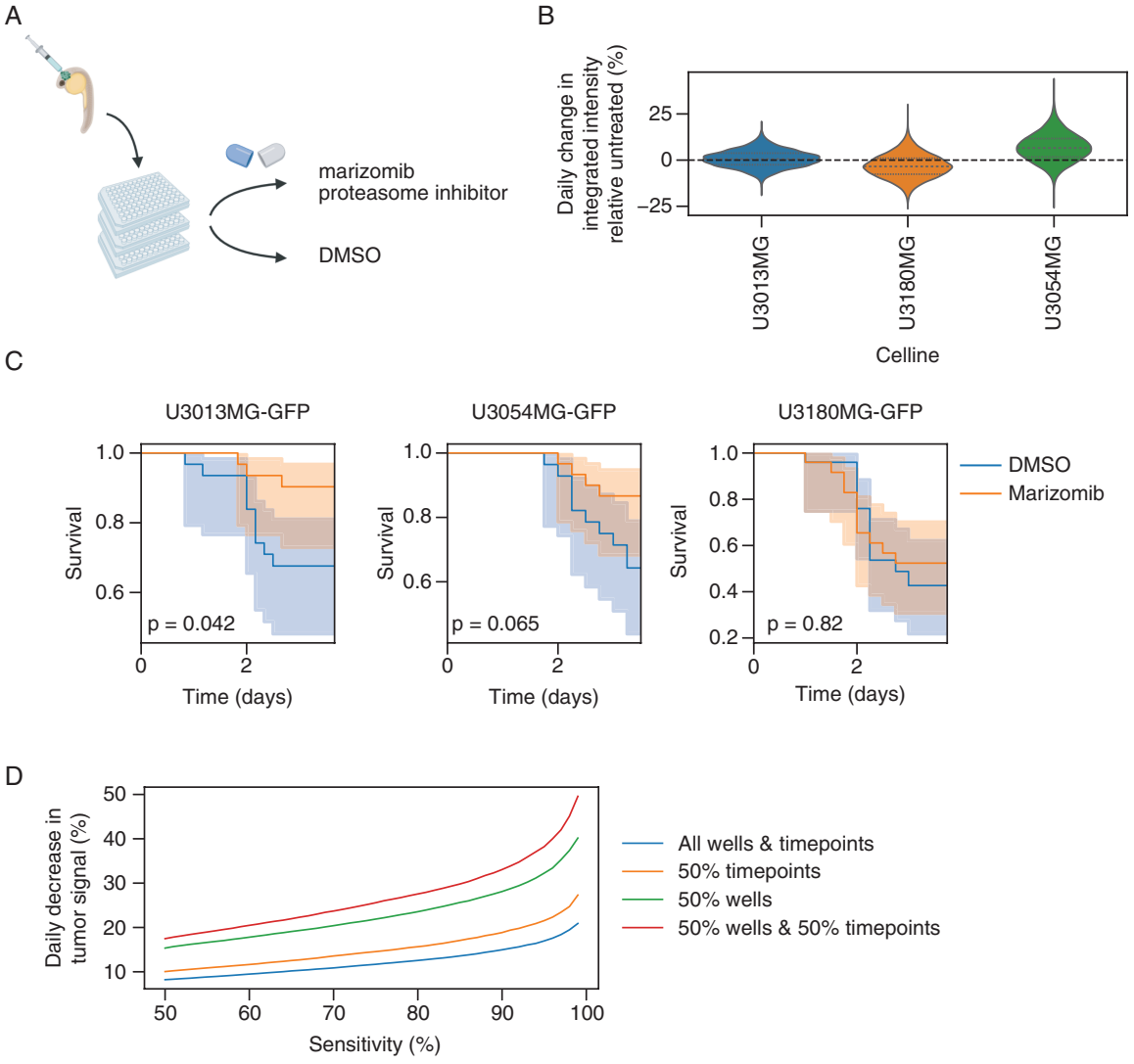

Figure 5. Heterogeneous treatment response is recapitulated in zebrafish xenografts of glioblastoma. (A) Treatment overview. (B) Posterior distribution of *in vivo* treatment effects for marizomib, compared with untreated, for three PDCs. (C) Survival benefit for treated fish using a Cox model (zones = 95% CI). (D) Power analysis of the zebrafish treatment model.

tumor signal would be correctly identified in 95% potential treatments (given alpha = 5%) (Figure 5D). Artificially decreasing the number of fish and timepoints by 50% increased the required effect size to 32% and 22% respectively. This highlights the importance of managing biological variability but if the technology is available, increasing image frequency is a cost-effective way of increasing power.

Discussion

Meeting the need for high-throughput *in vivo* models of glioblastoma, we developed a 5-day zebrafish orthotopic xenograft assay, in which time-lapse imaging and convolutional neural networks enable longitudinal observation of tumor development. Extending previous zebrafish assays, our model enables the joint measurement of patient-specific growth rate, survival time, tumor invasion, and response to treatment.

Our method offers a number of potential advantages over existing zebrafish-based methods. First, it involves very little animal handling as the only intervention is the injection, which trained staff can perform at a rate of around 300 fish per day. Compared to genetic zebrafish models of glioblastoma,[42,43] our model has a homogenous tumor onset and fish can be treated simultaneously. Further, longitudinal measurements control for variations due to the number of cells injected in individual fish. Endpoint measurements ignore this source of variation,[23] while some correct for this using two or more image time points.[16,17] In this study, we instead increased the temporal resolution to assess proper growth (and survival) for individual fish.

We found that GBM cells invaded larger anatomical structures including ventricles and midbrain/hindbrain boundary, but also invaded nuclear dense areas of the brain, suggesting an integration into the brain rather than a restricted local expansion (Supplementary Figure 6A–C, Supplementary Videos 12, 13). A subpopulation of invading cells was associated with blood vessels, and was more prominent in some PDCs than in others, in line with previous studies on GBM-vessel interactions in zebrafish.[44]

Our CNN-based image analysis method robustly deals with the problem of removing autofluorescence from the egg yolk, a common cause of false positives in GFP experiments in zebrafish. The pipeline is easily transferable to other zebrafish xenograft models making use of the IncuCyte (or equivalent) live-imaging instrumentation. The training set, model, and code used in this study is distributed freely (https://github.com/sven-nelander/zbt-seg).

We found that the proteasome inhibitor marizomib increased survival for PDC cultures sensitive to proteasome inhibition, indicating that our model will be useful for patient-specific drug testing. The presence of a survival effect without a reduction in GFP-signal could be due to the treatment affecting not only cell number but other pathophysiological interactions with the normal brain. For instance, in *Drosophila*, secretion of ImpL2, an antagonist of insulin signaling, by malignant tumors drives loss of normal tissue.[45] A second possibility is that cytokines produced by the tumor lead to activation of JAK/STAT signaling, inflammation, disruption of the blood-brain barrier, and reduced survival.[46] A third possibility is that marizomib, which suppresses invasion of GBM cells[47] reduces the infiltration of sensitive anatomical structures. Interestingly, the effect on survival for different PDC cultures was larger than could be attributed to changes in cell proliferation alone, which further underlines that additional effects beyond tumor mass are important for survival, reserved for future work.

The assay time of 72 hours suffices to generate a diversity of phenotypes between PDCs, indicating a potential to use specific cultures to investigate specific aspects of GBM in the zebrafish host. The five best performing PDC cultures (U3013MG, U3054MG, U3179MG, U3291MG, U3180MG) provide a concrete panel of PDCs for zebrafish-based evaluation of drugs with tumor growth, invasion, or survival endpoints. We recommend U3013MG as a robust choice of a fast-growing PDC, and U3179MG and U3180MG as particularly well suited for studies of invasion. One implication of the present study is thus that our model may find uses in analysis of pathways linked to GBM invasion, such as ephrin B2 signaling,[48] *SOX10*-driven gene expression[49],and Wnt7 signaling.[41] As is the case for all xenograft models, our model should be used with the awareness that xenografts may not reflect the full complexity of the disease as manifested in patients. Also, while 72 hours is a common time window in pharmacological experiments, some classes of drugs may need even longer times to yield effects. We are currently working on extensions of our method with longer treatment times.

All cultures are distributed as part of the HGCC resource. Data for each cell culture (mutations, gene expression profiles, methylomes, drug response) are available at portal.hgcc.se. Information for cell culture requests is found at hgcc.se. We expect our proposed method to facilitate and accelerate the *in vivo* evaluation of new therapies, specifically in regards to their effect on proliferation, invasion, and vessel interaction, which are all key malignant phenotypes of GBM. Follow-up studies will aim to extend the treatment window to further increase the potential of the model.

Supplementary Material

Supplementary material is available at *Neuro-Oncology* online.

Keywords

convolutional neural network | patient-derived xenografts | perivascular invasion | precision medicine | 3R

Acknowledgments

We thank the Human Glioma Cell Culture consortium (hgcc.se) for the development of the cell cultures, Magnus Essand, Uppsala University for providing the GFP-luc lentiviral construct and Ludmila Elfineh, Soumi Kundu and Karl Holmberg-Olausson for creation and characterization of the GFP-luc mouse models. Figure 1A, 4A, 5A, and Supplementary Figure 5 were created with BioRender. We would also like to thank the Genome Engineering Zebrafish National Facility at Uppsala University for their kind help with embryo production.

Funding

This work was supported by Swedish Cancer Society (200839PjF); the Swedish Research Council (20180269); the Swedish Foundation for Strategic Research (BD15-0082); The Knut and Alice Wallenberg Foundation (2017.0144); Vetenskapsrådet (VR-MH-2016-01437); Swedish Cancer Society (20 1086 Pj).

Conflict of interest statement. The authors declare no conflicts of interest.

Authorship statement. E.A., E.R., and S.N. planned the study. E.A., M.G., N.H., and R.S. conducted the experiments. E.R. developed the image analysis pipeline and performed the statistical analysis. E.A. and E.R. wrote the first version of the manuscript. C.K. developed GFP-luc cell cultures, mouse xenograft models, and their characterization. M.G., E.A., and K.K. characterized vascular invasion, proliferation, and apoptosis of zebrafish xenografts. E.A. and E.R. contributed equally. S.N. guided the study.

References

1. da Hora CC, Schweiger MW, Wurdinger T, Tannous BA. Patient-derived glioma models: from patients to dish to animals. *Cells*. 2019;8(10):1177.
2. Lee J, Kotliarova S, Kotliarov Y, et al. Tumor stem cells derived from glioblastomas cultured in bFGF and EGF more closely mirror the phenotype and genotype of primary tumors than do serum-cultured cell lines. *Cancer Cell*. 2006;9(5):391–403.
3. Carlson BL, Pokorny JL, Schroeder MA, Sarkaria JN. Establishment, maintenance and in vitro and in vivo applications of primary human glioblastoma multiforme (GBM) xenograft models for translational biology studies and drug discovery. *Curr Protoc Pharmacol*. 2011;Chapter 14:Unit 14.16.
4. Joo KM, Kim J, Jin J, et al. Patient-specific orthotopic glioblastoma xenograft models recapitulate the histopathology and biology of human glioblastomas in situ. *Cell Rep*. 2013;3(1):260–273.
5. Patrizii M, Bartucci M, Pine SR, Sabaawy HE. Utility of glioblastoma patient-derived orthotopic xenografts in drug discovery and personalized therapy. *Front Oncol*. 2018;8:23.
6. Vik-Mo EO, Sandberg C, Olstorn H, et al. Brain tumor stem cells maintain overall phenotype and tumorigenicity after in vitro culturing in serum-free conditions. *Neuro Oncol*. 2010;12(12):1220–1230.
7. Xie Y, Bergström T, Jiang Y, et al. The human glioblastoma cell culture resource: validated cell models representing all molecular subtypes. *EBioMedicine*. 2015;2(10):1351–1363.
8. Yang L, Clarke MJ, Carlson BL, et al. PTEN loss does not predict for response to RAD001 (Everolimus) in a glioblastoma orthotopic xenograft test panel. *Clin Cancer Res*. 2008;14(12):3993–4001.
9. Astone M, Dankert EN, Alam SK, Hoeppner LH. Fishing for cures: the allure of using zebrafish to develop precision oncology therapies. *Npj Precis Oncol*. 2017;1(1):1–14.
10. Letrado P, de Miguel I, Lamberto I, Díez-Martínez R, Oyarzabal J. Zebrafish: speeding up the cancer drug discovery process. *Cancer Res*. 2018;78(21):6048–6058.
11. Costa B, Estrada MF, Mendes RV, Fior R. Zebrafish avatars towards personalized medicine—a comparative review between avatar models. *Cells*. 2020;9(2):293.
12. Fior R, Póvoa V, Mendes RV, et al. Single-cell functional and chemosensitive profiling of combinatorial colorectal therapy in zebrafish xenografts. *Proc Natl Acad Sci U S A*. 2017;114(39):E8234–E8243.
13. Usai A, Di Franco G, Colucci P, et al. A model of a zebrafish avatar for co-clinical trials. *Cancers*. 2020;12(3):677.
14. Zeng A, Ye T, Cao D, et al. Identify a blood-brain barrier penetrating drug-TNB using zebrafish orthotopic glioblastoma xenograft model. *Sci Rep*. 2017;7(1):14372.
15. White RM, Sessa A, Burke C, et al. Transparent adult zebrafish as a tool for in vivo transplantation analysis. *Cell Stem Cell*. 2008;2(2):183–189.
16. Welker AM, Jaros BD, Puduvalli VK, Imitola J, Kaur B, Beattie CE. Standardized orthotopic xenografts in zebrafish reveal glioma cell-line-specific characteristics and tumor cell heterogeneity. *Dis Model Mech*. 2016;9(2):199–210.
17. Wehmas LC, Tanguay RL, Punnoose A, Greenwood JA. Developing a novel embryo-larval zebrafish xenograft assay to prioritize human glioblastoma therapeutics. *Zebrafish*. 2016;13(4):317–329.
18. Hamilton L, Astell KR, Velikova G, Sieger D. A zebrafish live imaging model reveals differential responses of microglia toward glioblastoma cells in vivo. *Zebrafish*. 2016;13(6):523–534.
19. Baskaran S, Mayrhofer M, Kultima HG, et al. Primary glioblastoma cells for precision medicine: a quantitative portrait of genomic (in)stability during the first 30 passages. *Neuro Oncol*. 2018;20(8):1080–1091.
20. Johansson P, Krona C, Kundu S, et al. A patient-derived cell atlas informs precision targeting of glioblastoma. *Cell Rep*. 2020;32(2):107897.
21. Pollard SM, Yoshikawa K, Clarke ID, et al. Glioma stem cell lines expanded in adherent culture have tumor-specific phenotypes and are suitable for chemical and genetic screens. *Cell Stem Cell*. 2009;4(6):568–580.
22. Hogan BM, Bos FL, Bussmann J, et al. Ccbe1 is required for embryonic lymphangiogenesis and venous sprouting. *Nat Genet*. 2009;41(4):396–398.
23. Pudelko L, Edwards S, Balan M, et al. An orthotopic glioblastoma animal model suitable for high-throughput screenings. *Neuro Oncol*. 2018;20(11):1475–1484.
24. Almstedt E, Elgendy R, Hekmati N, et al. Integrative discovery of treatments for high-risk neuroblastoma. *Nat Commun*. 2020;11(1):71.
25. Baier H, Wullimann MF. Anatomy and function of retinorecipient arborization fields in zebrafish. *J Comp Neurol*. 2021;529(15):3454–3476.
26. Ronneberger O, Fischer P, Brox T. U-Net: convolutional networks for biomedical image segmentation. *arXiv*. 2015:1505.0459v1.
27. Chollet F, et al. Keras. 2015. https://keras.io.
28. Abadi M, Agarwal A, Barham P, et al. TensorFlow: large-scale machine learning on heterogeneous distributed systems. *ArXiv160304467 Cs*. 2016. http://arxiv.org/abs/1603.04467. Accessed April 9, 2020.
29. Davidson-Pilon C. Lifelines: survival analysis in Python. *J Open Source Softw*. 2019;4(40):1317.
30. Homan MD, Gelman A. The No-U-turn sampler: adaptively setting path lengths in Hamiltonian Monte Carlo. *J Mach Learn Res*. 2014;15(1):1593–1623.
31. Salvatier J, Wiecki TV, Fonnesbeck C. Probabilistic programming in Python using PyMC3. *PeerJ Comput Sci*. 2016;2:e55.
32. Kostaras X, Cusano F, Kline GA, Roa W, Easaw J. Use of dexamethasone in patients with high-grade glioma: a clinical practice guideline. *Curr Oncol*. 2014;21(3):e493–e503.
33. Koltowska K, Lagendijk AK, Pichol-Thievend C, et al. Vegfc regulates bipotential precursor division and prox1 expression to promote lymphatic identity in zebrafish. *Cell Rep*. 2015;13(9):1828–1841.
34. Le Guen L, Karpanen T, Schulte D, et al. Ccbe1 regulates Vegfc-mediated induction of Vegfr3 signaling during embryonic lymphangiogenesis. *Development*. 2014;141(6):1239–1249.
35. Schindelin J, Arganda-Carreras I, Frise E, et al. Fiji: an open-source platform for biological-image analysis. *Nat Methods*. 2012;9(7):676–682.
36. Segerman A, Niklasson M, Haglund C, et al. Clonal variation in drug and radiation response among glioma-initiating cells is linked to proneural-mesenchymal transition. *Cell Rep*. 2016;17(11):2994–3009.
37. Scherer HJ. Structural development in gliomas. *Am J Cancer*. 1938;34(3):333–351.
38. Seano G, Jain RK. Vessel co-option in glioblastoma: emerging insights and opportunities. *Angiogenesis*. 2020;23(1):9–16.
39. Cuddapah VA, Robel S, Watkins S, Sontheimer H. A neurocentric perspective on glioma invasion. *Nat Rev Neurosci*. 2014;15(7):455–465.
40. Liu CJ, Shamsan GA, Akkin T, Odde DJ. Glioma cell migration dynamics in brain tissue assessed by multimodal optical imaging. *Biophys J*. 2019;117(7):1179–1188.
41. Griveau A, Seano G, Shelton SJ, et al. A glial signature and Wnt7 signaling regulate glioma-vascular interactions and tumor microenvironment. *Cancer Cell*. 2018;33(5):874–889.e7.
42. Ju B, Chen W, Orr BA, et al. Oncogenic KRAS promotes malignant brain tumors in zebrafish. *Mol Cancer*. 2015;14:18.
43. Jung IH, Leem GL, Jung DE, et al. Glioma is formed by active Akt1 alone and promoted by active Rac1 in transgenic zebrafish. *Neuro Oncol*. 2013;15(3):290–304.

44. Umans RA, ten Kate M, Pollock C, Sontheimer H. Fishing for contact: modeling perivascular glioma invasion in the zebrafish brain. *ACS Pharmacol Transl Sci.* 2020;4(4):1295–1305.

45. Figueroa-Clarevega A, Bilder D. Malignant Drosophila tumors interrupt insulin signaling to induce cachexia-like wasting. *Dev Cell.* 2015;33(1):47–55.

46. Kim J, Chuang H-C, Wolf NK, et al. Tumor-induced disruption of the blood-brain barrier promotes host death. *Dev Cell.* 2021;56(19):2712–2721.e4.

47. Di K, Lloyd GK, Abraham V, et al. Marizomib activity as a single agent in malignant gliomas: ability to cross the blood-brain barrier. *Neuro Oncol.* 2016;18(6):840–848.

48. Krusche B, Ottone C, Clements MP, et al. EphrinB2 drives perivascular invasion and proliferation of glioblastoma stem-like cells. *Elife.* 2016;5:e14845.

49. Brooks LJ, Clements MP, Burden JJ, et al. The white matter is a pro-differentiative niche for glioblastoma. *Nat Commun.* 2021;12(1):2184.